[CANCER RESEARCH 64, 7773–7779, November 1, 2004]

Pten Loss Causes Hypertrophy and Increased Proliferation of Astrocytes *In vivo*

Melissa M. Fraser,[1] Xiaoyan Zhu,[1] Chang-Hyuk Kwon,[1,2] Erik J. Uhlmann,[3] David H. Gutmann,[3] and Suzanne J. Baker[1]

[1]Department of Developmental Neurobiology, St. Jude Children's Research Hospital, Memphis, Tennessee; [2]Center for Developmental Biology, University of Texas Southwestern Medical Center of Dallas, Dallas, Texas; and [3]Department of Neurology, Washington University School of Medicine, St. Louis, Missouri

ABSTRACT

Somatic mutations of *PTEN* are found in many types of cancers including glioblastoma, the most malignant astrocytic tumor. *PTEN* mutation occurs in 25 to 40% of glioblastomas but is rarely observed in low-grade glial neoplasms. To determine the role of Pten in astrocytes and glial tumor formation, we inactivated *Pten* by a Cre-loxP approach with a *GFAP-cre* transgenic mouse that induced Cre-mediated recombination in astrocytes. *Pten* conditional knockout mice showed a striking progressive enlargement of the entire brain. Increased nuclear and soma size was observed in both astrocytes and neurons, which contributed in part to the increase in brain size. Pten-deficient astrocytes showed accelerated proliferation *in vitro* and aberrant ongoing proliferation in adult brains *in vivo*. In contrast, neurons lacking Pten did not show alterations in proliferation. This study shows cell-type dependent effects of Pten loss in the adult brain, including increased astrocyte proliferation that may render astroglial cells susceptible to neoplastic transformation or malignant progression.

INTRODUCTION

PTEN plays an important role in growth regulation relevant to tumorigenesis as well as in the normal development of multiple tissues. As a tumor suppressor gene, *PTEN* is frequently inactivated by somatic mutation in sporadic tumors of the brain, endometrium, and prostate, and with lower frequency in other tumor types (1). Inherited *PTEN* mutation results in cancer predisposition in breast, thyroid, and endometrial tissues. In addition, developmental abnormalities, including hamartomas in multiple tissues, enlarged brain size (macrocephaly), seizures, ataxia, mental retardation, and a cerebellar growth disorder termed Lhermitte-Duclos disease also occur. The penetrance of these inherited abnormalities is highly variable, leading to a wide range of disease severity associated with germline *PTEN* mutation (2).

PTEN is a lipid phosphatase that dephosphorylates the 3′ position of both phosphatidylinositol 3,4,5-triphosphate and phosphatidylinositol 4,5-bisphosphate. This activity directly reverses the phosphorylation catalyzed by phosphatidylinositol 3′-kinase (PI3k), thereby placing PTEN as a central negative regulator of the phosphatidylinositol 3′-kinase pathway (3). PTEN is believed to exert its tumor suppressor activity predominantly through negative regulation of the growth, proliferative, and survival signals transduced through phosphatidylinositol 3′-kinase pathway signaling. Consistent with this hypothesis, the vast majority of *PTEN* mutations observed in human tumors ablate PTEN lipid phosphatase activity (4). Intriguingly, there are additional PTEN functions, which may be independent of its lipid phosphatase activity, including negative regulation of p53 and inhibition of glioma cell migration (5, 6).

The critical role of Pten in development is underscored by the embryonic lethality observed in Pten-null mice at approximately day E7.5 (7–9). These *Pten*-deficient embryos exhibit abnormal placental formation and patterning defects in the cephalic and caudal regions. To gain insights into the role of Pten in specific tissues and to circumvent the embryonic lethality observed in conventional knockout mice, Cre/loxP-mediated *Pten* inactivation has been used to dissect the complex and context-dependent roles performed by Pten in development, homeostasis, and tumor suppression (4). These studies indicate several fundamental cellular processes for which Pten is required, including cell migration during development, regulation of cell size, proliferation, and apoptosis. Loss of Pten, however, does not interfere with cell fate determination.

In the nervous system, deletion of *Pten* in neural progenitor cells during embryogenesis disrupts migration and proper formation of the laminar structure of the brain (10, 11). Depending on the specific population of cells targeted for *Pten* deletion, Pten loss is associated with both increases and decreases in proliferation and apoptosis. Postnatal deletion of *Pten* in selective neuronal populations resulted in dramatic increases in neuronal soma size without alterations in proliferation (12, 13). Taken together, these studies with conditional knockout mice have shown that Pten loss results in disrupted regulation of cell size or cell number in the brain and underscore the importance of Pten in normal central nervous system development and maintenance.

Tumorigenesis resulting from Pten loss has been shown in a number of diverse tissues in mouse. For example, Pten loss is associated with increased proliferation of T-cells, B-cells, keratinocytes, prostate epithelium, and mammary epithelium. Tumorigenesis is observed in both *Pten*+/− mice and *Pten* conditional knockout models, in which mice develop endometrial, lymphoid, thyroid, liver, testicular, breast, skin, and prostate cancers (7–9, 14–19). In contrast, less is known about the function of Pten in astrocytic tumorigenesis. In glioblastomas, *PTEN* mutations are found in combination with mutations in other genes including *p53*, *INK4A/ARF*, and *EGFR* (20), and it is unclear which aspects of PTEN dysfunction contribute to glioblastoma formation. Because glioblastomas are believed to arise from an astrocyte or astrocyte precursor cell, we generated mice in which *Pten* was conditionally deleted in astrocytes. Here we show that Pten loss causes hypertrophy and hyperproliferation of cortical astrocytes. These results suggest that Pten plays a central role in modulating cell size and growth relevant to astroglial cell tumorigenesis in the nervous system.

MATERIALS AND METHODS

Transgenic Mice. *GFAP-cre* transgenic mice were described previously (21), and they were used to drive *cre* recombinase expression in the nervous system of the mouse. *GFAP-cre* mice were bred with *ROSA26R* (22) mice to map *in vivo* cre activity. Cre activity was detected by X-gal staining frozen sagittal tissue sections. *GFAP-Cre* mice were bred with $Pten^{loxP/loxP}$ (23), a gift from Tak Mak (University of Toronto, Toronto, Ontario, Canada), to generate

Received 7/12/04; revised 8/27/04; accepted 9/13/04.

Grant support: NIH Grants NS44172, CA096832 (S. Baker), and NS41097 (D. Gutmann), the American Lebanese Syrian Associated Charities, and the United States Army (DAMD17-03-1-0073; D. Gutmann).

The costs of publication of this article were defrayed in part by the payment of page charges. This article must therefore be hereby marked *advertisement* in accordance with 18 U.S.C. Section 1734 solely to indicate this fact.

Note: C.-H. Kwon is currently in the Center for Developmental Biology, University of Texas Southwestern Medical Center of Dallas, Dallas, Texas. Supplementary data for this article may be found at Cancer Research Online at http://cancerres.aacrjournals.org.

Requests for reprints: Suzanne J. Baker, Department of Developmental Neurobiology, St. Jude Children's Research Hospital, 332 North Lauderdale, Memphis, TN 38105. Phone: (901) 495-2254; Fax: (901) 495-2270; E-mail: Suzanne.Baker@stjude.org.

Pten conditional knockout mice, *Pten*$^{loxP/loxP}$;*GFAP-Cre*. No abnormalities were observed in *Pten*$^{+/+}$;*GFAP-Cre, Pten*$^{+/loxP}$;*GFAP-Cre*, or *Pten*$^{loxP/loxP}$;*No cre* mice. For *in vivo* bromodeoxyuridine (BrdU) labeling, mice received injections every two hours with 50 μg of BrdU per gram of body weight for 5 injections. Mice were euthanized 2 hours after the last injection.

Immunohistochemistry. Mice were transcardially perfused with 2% paraformaldehyde in PBS. All tissues were postfixed in 2% paraformaldehyde overnight. For X-gal staining, tissues were equilibrated in 25% sucrose in PBS for an additional 24 hours, then cryosectioned at a thickness of 12 μm, and stained with X-gal. For paraffin sections, tissues were postfixed for an additional 24 hours in 4% paraformaldehyde, embedded in paraffin, and cut into 5-μm sections. Littermate controls were perfused and processed at the same time as the matched conditional knockout animals and were of the genotypes *Pten*$^{+/+}$*;GFAP-cre* or *Pten*$^{+/+}$ or *Pten*$^{loxP/loxP}$ without cre. We performed immunohistochemistry with primary antibodies to BrdU (10 μg/mL; Biodesign), Gfap (1:1000 for immunohistochemistry, 1:200 for immunofluorescence; Sigma, St. Louis, MO), Mac1 (1:50; PharMingen, San Diego, CA), Nestin (1:50; Chemicon, Temecula, CA), NeuN (1:500; Chemicon), Phosphoser 473-Akt (1:50; Cell Signaling, Beverly, MA), Pten (1:50; NeoMarkers, Freemont, CA), S100β (1:1,000 for immunohistochemistry, 1:200 for immunofluorescence; Sigma), S100 (1:100; Dako, Carpinteria, CA), and Map-2 (1:5,000; Sternberger Monoclonals, Inc., Lutherville, MD). We used microwave antigen retrieval for all of the antibodies except S100β. We used fluorescein isothiocyanate or cyanine 3-conjugated secondary antibodies (Jackson ImmunoResearch, West Grove, PA) for immunofluorescence. For immunohistochemistry, we used biotin-labeled secondary antibody detected by peroxidase-conjugated avidin (Elite ABC, Vector Laboratories, Burlingame, CA) treated with 3,3′-diaminobenzidine substrate, and counterstained with hematoxylin (Vector Laboratories). Coimmunodetection of BrdU with other proteins was performed sequentially as described previously (24). Cresyl violet staining was carried out per standard protocol with 0.02% working solution of cresyl violet. Levels of apoptosis were analyzed by terminal deoxynucleotidyl transferase-mediated nick end labeling (TUNEL) staining with the ApopTag fluorescein *in situ* apoptosis detection kit (Chemicon) per the manufacturer's protocol. The 4′,6-diamidino-2-phenylindole stain was performed with Vectashield mounting media (Vector Laboratories).

Cell Counts and Measurements. The Bioquant system (Bioquant Image Analysis Corp., Nashville, TN) was used to determine the number of BrdU-positive, S100-positive, and NeuN-positive cells in the cerebral cortex of the animals. Three sets of matched sagittal sections were obtained, and immunodetection with BrdU (Biodesign), NeuN (Chemicon), or S100 (Dako) was used to detect proliferating cells, neurons, or glia, respectively. Using Bioquant, the area of the cerebral cortex that lies dorsal to the hippocampal formation was outlined, and the cells within this area that were positive for BrdU, NeuN, or S100 were counted. For each antibody, positive cells were counted from 3 sections from each brain, and 3 control and 3 *Pten*$^{loxP/loxP}$;*GFAP-Cre* brains were analyzed for each age. The Bioquant system was also used to estimate astrocyte soma size by outlining individual astrocyte soma in the corpus callosum from cells that contained a nucleus in the plane of section. Greater than 100 cells were measured from Gfap immunostained slides from control ($n = 3$) or *Pten*$^{loxP/loxP}$;*GFAP-Cre* ($n = 3$) mice.

Primary Astrocyte Cultures and Analysis of Growth. Cortical astrocyte cultures were established from postnatal day 2 mice. Tissue from the cerebral cortex was cut into small pieces, and either digested in a 1:1 mixture of DMEM and trypsin/EDTA solution for 15 minutes at 37°C or mechanically disaggregated without trypsin. Tail DNA was used to determine the genotype of each animal. Astrocytes were seeded as separate cultures (passage 0) in Primaria T25 flasks in DMEM supplemented with 10% FCS, 20 ng/mL mouse epidermal growth factor (E-4127, Sigma), 50 mg/mL penicillin, and 50 mg/mL streptomycin until subconfluent (day 5), then trypsinized and replated in Primaria (Falcon, San Jose, CA) T75 flasks (passage 1). On day 8, 4×10^4 cells were seeded in 35-mm dishes (passage 2). Triplicate dishes were seeded and counted for cultures established from each mouse. Cells were trypsinized, and the number of trypan blue-excluding cells was determined by direct counting in a hemocytometer in triplicate on days 9 to 14. Numbers were plotted as cells per square centimeter growth area.

Southern Blot Analysis. Genomic DNA was extracted from mouse tails, and primary astrocyte cultures, digested with *Hind*III, were separated by electrophoresis in a 1% agarose gel and transferred to Hybond-N$^+$ nylon filter by alkaline transfer. A 380-bp fragment of *Pten* intron 3 (13) was used to detect the wild-type, floxed, and cre-mediated deletion of the floxed *Pten* locus.

Western Blot Analysis. Protein was extracted from primary cerebral cortical astrocyte cultures with Cell Lysis Buffer (Cell Signaling) containing 10 mmol/L sodium fluoride, 1 mmol/L sodium orthovanadate, and protease inhibitor cocktail (Roche, Indianapolis, IN). Protein samples (15 μg) were resolved on a 4 to 12% gradient Bis-Tris gel and transferred to nitrocellulose. Proteins were detected with antibodies against Pten (1:500; NeoMarkers), P-Akt (1:1,000; P-Ser 473, Cell Signaling), or β-actin (1:2,500; Sigma) and visualized with peroxidase-conjugated secondary antibodies and Super Signal chemiluminescent detection (Pierce, Rockford, IL).

RESULTS

***GFAP-cre* Mice Exhibit Cre-Mediated Recombination in Astrocytes and a Subset of Neurons.** To selectively delete *Pten* in the mouse central nervous system, we used *GFAP-cre* transgenic mice, in which the human glial fibrillary acidic protein (*GFAP*) promoter directs expression of a bicistronic message comprising *cre* recombinase, an internal ribosome entry site and a *lacZ* reporter gene (21). Previous characterization of these *GFAP-cre* mice showed that Cre and β-galactosidase were coexpressed selectively in astrocytes and not in neurons, with expression detected at E14.5, consistent with the expected expression pattern for the *GFAP* promoter. No expression was observed outside the central nervous system (21). Because Cre recombinase irreversibly deletes segments of DNA flanked by loxP sites, the current expression of a *cre* transgene may give an incomplete indication of the accumulated Cre-mediated excision within a tissue. We bred *GFAP-cre* mice with *ROSA26R* reporter mice to accurately assess the extent of Cre-mediated recombination. These reporter mice express the *lacZ* reporter gene constitutively only after Cre-mediated recombination occurs (22). The *lacZ* expression in *GFAP-cre* mice (Fig. 1, *A* and *C*) shows the current *GFAP-cre* transgene expression, whereas *lacZ* expression in *GFAP-cre;ROSA26R* mice reveals a much greater number of cells in which Cre-mediated deletion occurred (Fig. 1, *B* and *D*). There was no detectable reporter expression in brains from *ROSA26R* mice without the *cre* transgene (data not shown).

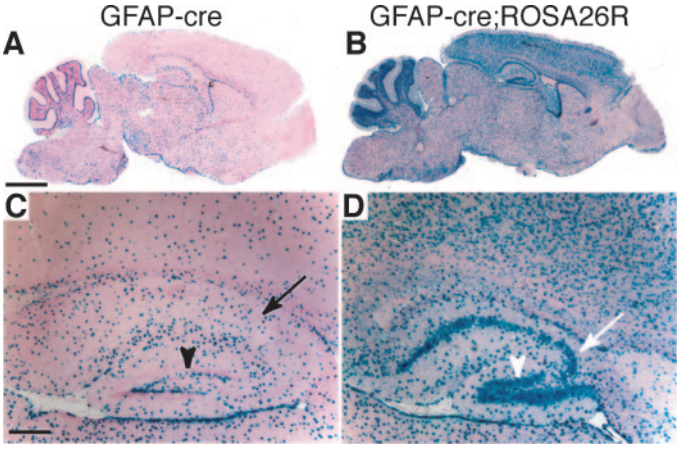

Fig. 1. *GFAP-cre* transgene expression and extent of Cre-mediated recombination. The *GFAP-cre* transgene contains an internal ribosome entry site and a *lacZ* reporter to allow identification of transgene expression from the *GFAP* promoter (*left panels*, *A* and *C*). *GFAP-cre* mice were crossed with *ROSA26R* mice, where Cre-mediated recombination is necessary for the constitutive expression of the β-galactosidase reporter (*right panels*, *B* and *D*). Current Cre expression (*left panels*) or cells in which Cre-mediated excision has occurred (*right panels*) in 4-week-old mice are shown by X-gal staining (*blue*) and nuclear fast red counter stain (*pink*; *A–D*). *A* and *B*. Low magnification of *GFAP-cre* mice compared with *GFAP-cre;ROSA26R* mice are shown. *C* and *D*. Transgene expression is undetectable in neurons of the hippocampus (*arrow*) and the dentate gyrus (*arrow head*), but extensive Cre-mediated recombination in these neuronal populations is revealed by reporter expression in the nuclei of pyramidal (*arrow*) and granule (*arrow head*) neurons (*D*). *Scale bar* = 1.6 mm for *A* and *B* and 300 μm for *C* and *D*.

Expression of the Cre reporter was detected in neuronal populations that lacked expression of the *GFAP-cre* transgene. For example, whereas there was no detectable expression of the transgene in select neuronal populations in the dentate gyrus and hippocampus (Fig. 1*C*), Cre reporter expression showed extensive Cre-mediated recombination in these neuronal populations (Fig. 1*D*). The most striking examples of neuronal Cre-mediated recombination occurred within the hippocampal region and the granule neurons of the cerebellum, with less Cre-mediated recombination in other neuronal populations throughout the brain (Fig. 1*B*). *GFAP-cre* mice bred with an alternative Cre reporter mouse, *Z/EG* (25), confirmed the presence of Cre-mediated deletion in astrocytes as well as neurons (data not shown).

Pten Loss in Astrocytes and Neurons of *Pten*$^{loxP/loxP}$;*GFAP-Cre* Mice. We crossed *GFAP-cre* mice with *Pten*^{loxP} mice (23) to selectively inactivate *Pten* in astrocytes and neurons. Loss of Pten expression was observed throughout the brain in cell populations, consistent with the Cre reporter expression shown in *GFAP-cre;ROSA26R* mice. For example, loss of Pten expression was observed in the hippocampal region of mutant mice compared with control mice, including many pyramidal neurons in the hippocampus and granule neurons of the dentate gyrus (Fig. 2*A*). Previous studies showed that Pten loss was typically associated with an increase in cellular levels of phosphatidylinositol 3,4,5-triphosphate and a resulting increase in the phosphorylation and activation of the downstream effector Akt (4). As expected, minimal levels of phosphorylated Akt were observed in control mice, compared with a dramatic increase in phosphorylated Akt that corresponded to Pten loss in the *Pten*$^{loxP/loxP}$;*GFAP-Cre* mice (Fig. 2*B*). Pten loss was clearly detectable but less widespread in the cerebral cortex (Fig. 2C), consistent with the Cre reporter expression observed in the *GFAP-cre;ROSA26R* mice (Fig. 1). To show *Pten* deletion in astrocytes, we established primary cortical astrocyte cultures. Southern blot analysis showed virtually complete Cre-mediated deletion of the *Pten*^{loxP} allele within astrocytes from *Pten*$^{loxP/loxP}$;*GFAP-Cre* mice, compared with DNA extracted from tail where Cre recombinase was not active (Fig. 3*A*, *Lanes 5–7* compared with *Lane 2*). As expected, *Pten*$^{loxP/loxP}$;*GFAP-Cre* astrocytes showed a loss of Pten protein expression and a corresponding increase in phosphorylated Akt (Fig. 3*B*). Therefore, *Pten*$^{loxP/loxP}$;*GFAP-Cre* mice showed *Pten* inactivation in astrocytes as well as subsets of neuronal populations, as predicted from the *GFAP-cre;ROSA26R* reporter expression.

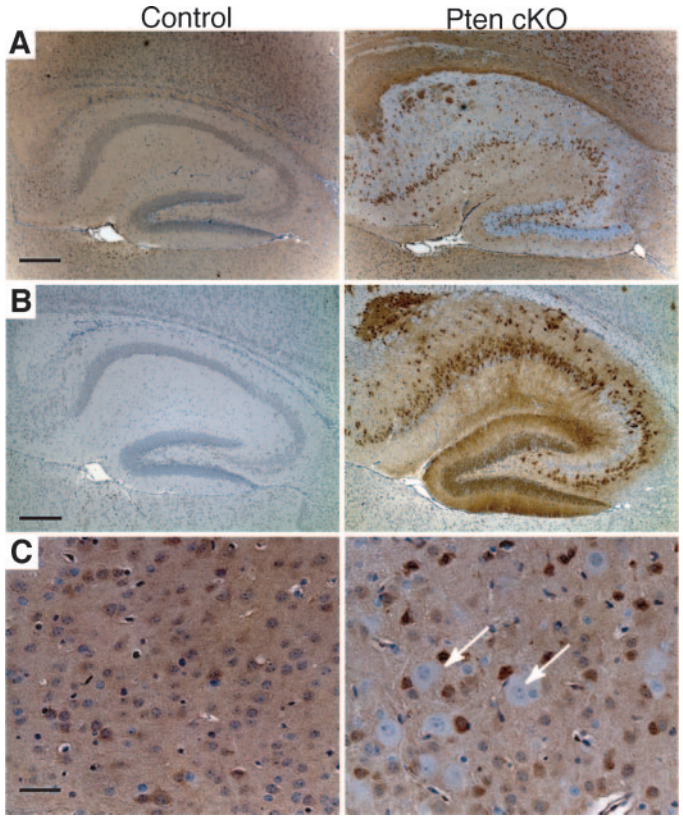

Fig. 2. Pten loss in *Pten*$^{loxP/loxP}$;*GFAP-Cre* mice. Immunostains of the hippocampal region (*A* and *B*) and cerebral cortex (*C*) from control (*left panels*) and *Pten*$^{loxP/loxP}$;*GFAP-Cre* (*right panels*) mice at P14. *A*. Pten immunodetection shows loss of Pten expression in the majority of cells in the hippocampal region of *Pten*$^{loxP/loxP}$;*GFAP-Cre* mice compared with control mice. *B*. Phosphorylated Akt immunodetection was observed in areas with loss of Pten expression in *Pten*$^{loxP/loxP}$;*GFAP-Cre* mice. There are no detectable levels of phosphorylated Akt in the hippocampal region of control animals. *C*. Pten immunohistochemistry in the cerebral cortex showed less extensive deletion of Pten (*arrows*) than observed in the hippocampal region. *Scale bar* = 300 μm for *A* and *B* and 40 μm for *C*.

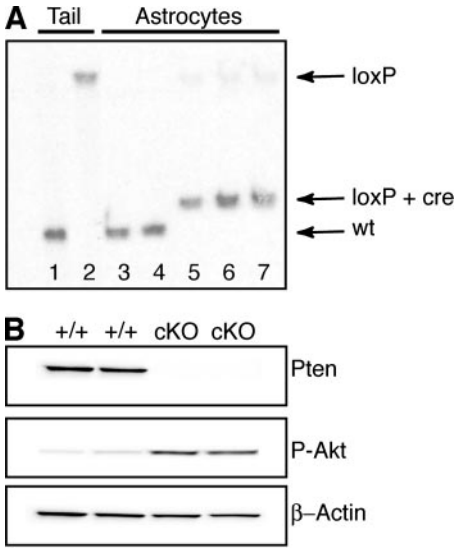

Fig. 3. Deletion of *Pten* in astrocytes. *A*. Southern blot detection showed cre-mediated deletion of Pten in the vast majority of astrocytes. DNA was extracted from wild-type (*Lanes 1*, *3*, and *4*) or conditional knockout mice (*Lanes 2* and *5–7*), from the tail (*Lanes 1* and *2*) or primary cortical astrocyte cultures established from postnatal day 2 mice (*Lanes 3–7*). Southern blot analysis of *Hind*III digested DNA with a *Pten*-specific probe shows the wild-type (*wt*) allele and the targeted *Pten*^{loxP} allele before (*loxP*) and after (*loxP + cre*) cre-mediated deletion. *B*. Pten loss is associated with an increase in phospho-Akt in astrocytes. Extracts from primary astrocyte cultures established from *Pten*$^{+/+}$;*GFAP-cre* (*+/+*) and *Pten*$^{loxP/loxP}$;*GFAP-Cre* (*cKO*) mice were analyzed by Western blot with anti-Pten, anti-phospho-Akt (Ser 473), and anti-β-actin. β-Actin is shown as a loading control.

Decreased Survival Rates in *Pten*$^{loxP/loxP}$;*GFAP-Cre* Mice. *Pten*$^{loxP/loxP}$;*GFAP-Cre* mice were phenotypically indistinguishable from their littermate controls at birth. However, *Pten*$^{loxp/loxp}$;*GFAP-cre* mice died prematurely compared with control mice. Fifty-two control and 49 *Pten*$^{loxP/loxP}$;*GFAP-Cre* mice were observed over a period of 160 days (Supplemental Fig. 1). Forty percent of the *Pten*$^{loxP/loxP}$;*GFAP-Cre* mice died before reaching 50 days of age; however, mutant mice that survived past 50 days had similar life spans to those of the control group during the observation period. In the mice that died prematurely, enlarged domed-shaped heads and ataxia were detectable by 3 weeks of age, and a similar phenotype developed later in the surviving mutant mice. Seizures were observed in ~20% of mutant mice, with an average onset at 10 weeks of age. The difference in survival between the two cohorts of *Pten*$^{loxP/loxP}$;*GFAP-Cre* mice may reflect the influence of different genetic backgrounds within the mouse colony (FVB/C57Bl/129).

Enlarged Neurons and Astrocytes Contribute to the Brain Hypertrophy Seen in *Pten*$^{loxP/loxP}$;*GFAP-Cre* Mice. Previous *Pten* conditional knockout models have shown disrupted neuronal migration during development with varying severity, which reflects the

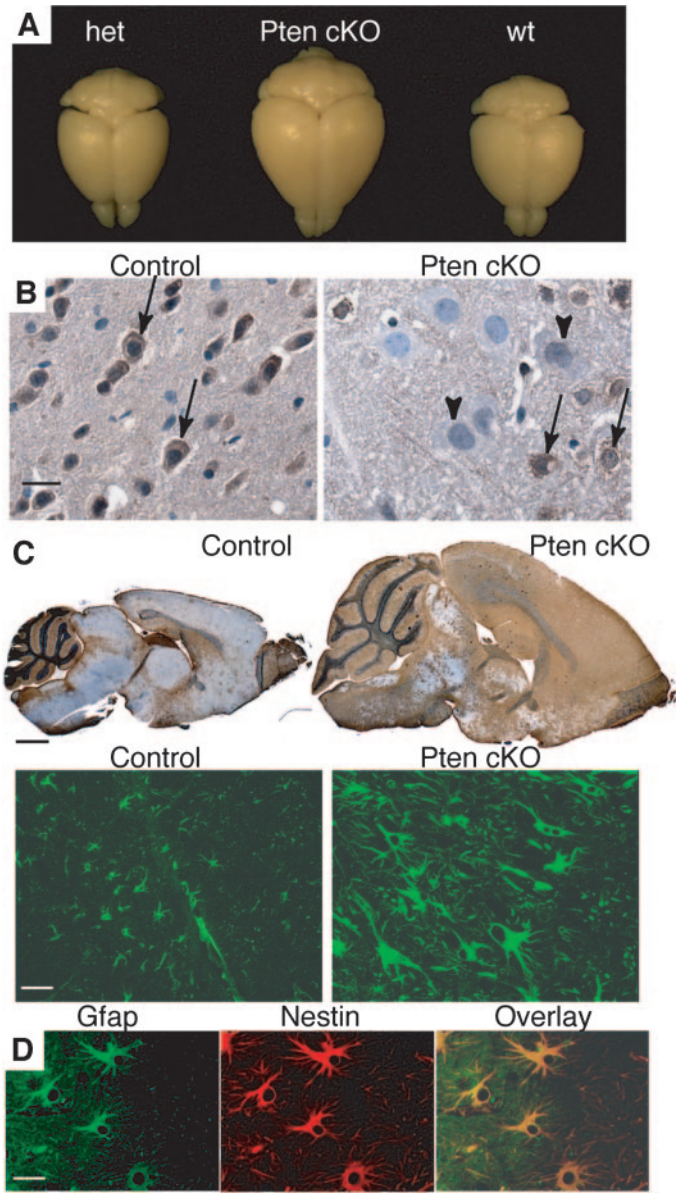

Fig. 4. Hypertrophy in *Pten*$^{loxP/loxP}$;*GFAP-Cre* brains. *A*. *Pten*$^{loxP/loxP}$;*GFAP-Cre* (*Pten cKO*) brains are enlarged compared with wild-type (*wt*) and *Pten*$^{+/loxP}$;*GFAP-cre* (*het*) littermates. *B*. Pten immunodetection in the cerebral cortex from adult control (*left*) and *Pten*$^{loxP/loxP}$;*GFAP-Cre* (*Pten cKO*) mice. Neurons expressing Pten in control and *Pten*$^{loxP/loxP}$;*GFAP-Cre* mice have similar sizes (*arrows*), whereas neurons that lost Pten expression (*arrow heads*) have cell autonomous enlargement of both the nucleus and cytoplasm. *C*. Gfap immunohistochemistry shows an overall increase in Gfap in *Pten*$^{loxP/loxP}$;*GFAP-Cre* brains (*C*, *top right*) compared with control (*C*, *top left*). Gfap immunofluorescence shows enlarged astrocytes in the cerebral cortex of *Pten*$^{loxP/loxP}$;*GFAP-Cre* mice (*C*, *bottom right*) compared with control (*C*, *bottom left*) shown at the same magnification. *D*. Reactive astrocytes that coexpress Gfap (*green*) and Nestin (*red*) were occasionally observed in focal areas in *Pten*$^{loxP/loxP}$;*GFAP-Cre* brains. Dentate gyrus from an adult mouse that experienced multiple seizures is shown. Overlay of the Gfap and Nestin immunofluorescence is shown. *Scale bar* = 20 μm for *B*, 1.25 mm for *top panels* in *C*, 50 μm for *bottom panels* in *C*, and 30 μm for *D*.

developmental timing of *Pten* inactivation and the particular cell populations affected (10–13). Similarly, we observed developmental abnormalities in the laminar organization of neurons because of incomplete neuronal migration in the hippocampus and cerebellum (Supplemental Fig. 2). In addition, we observed abnormalities acquired in aging animals after normal brain development was complete. Gross examination showed an overall enlargement of the entire brain of adult *Pten*$^{loxP/loxP}$;*GFAP-Cre* mice compared with *Pten*$^{+/loxP}$;*GFAP-cre* or wild-type controls (Fig. 4*A*). Macrocephaly of *Pten* conditional knockout mice increased progressively with age (Supplemental Fig. 3*A*). Previous studies in which *Pten* was selectively deleted in specific neuronal populations showed hypertrophy caused by a cell autonomous increase in nuclear and soma size of Pten-deficient neurons (12, 13). Consistent with these earlier studies, Pten-expressing neurons in control or *Pten*$^{loxP/loxP}$;*GFAP-Cre* mice maintained a similar size, whereas Pten-deficient neurons in *Pten*$^{loxP/loxP}$;*GFAP-Cre* mice showed a substantial increase in both nuclear and soma size (Fig. 4*B*). This cell-autonomous hypertrophy was observed in Pten-deficient neurons throughout the brain including the cerebral cortex, hippocampal region, and cerebellum. To assess the effect of Pten loss on astrocytes, we visualized astrocytes by immunohistochemistry for Gfap, an astrocyte marker. Compared with controls, there was a dramatic increase in the number of cells expressing Gfap throughout the enlarged *Pten*$^{loxP/loxP}$;*GFAP-Cre* brains (Fig. 4*C*, sagittal sections). Such an increase in Gfap immunoreactivity could indicate an increase in the number of astrocytes or reactive astrocytosis, a process that occurs after insult or injury, characterized by hypertrophic astrocytes and enhanced Gfap immunoreactivity with or without proliferation (26). A higher magnification view of Gfap immunofluorescence clearly demonstrates dramatic enlargement of astrocytes in *Pten*$^{loxP/loxP}$;*GFAP-Cre* mice compared with control mice (Fig. 4*C*, *bottom panels*; Supplemental Fig. 3*B*). Astrocyte hypertrophy was detectable by 4 weeks of age and increased progressively with age. An additional feature of reactive astrocytes is coexpression of nestin, a marker normally expressed in neural progenitor cells, along with Gfap (27). The vast majority of Gfap-expressing cells in *Pten*$^{loxP/loxP}$;*GFAP-Cre* brains did not express nestin (data not shown). However, there were focal areas in some adult *Pten*$^{loxP/loxP}$;*GFAP-Cre* brains that contained reactive astrocytes. These cells were hypertrophic, coexpressed nestin and Gfap (Fig. 4*D*) and, in some cases, showed proliferation as well as occasional binucleated cells (data not shown). Reactive astrocytes were limited to damaged regions, including the hippocampal formation of an animal that had frequent seizures, and showed substantial neuronal death in this region, as well as in areas of the cerebellum immediately adjacent to the skull, in which brain enlargement was likely to cause parenchymal compression. Reactive astrocytosis is also sometimes accompanied by microgliosis, an immune response by microglia within the brain. However, microglia, identified by Mac-1 immunopositivity, were only rarely observed in the hippocampal region in a few animals that had experienced seizures (data not shown). Thus, Pten-deficiency caused a substantial enlargement in both neurons and astrocytes. The massive hypertrophy of astrocytes in *Pten*$^{loxp/loxp}$;*GFAP-cre* mice was distinct from areas of reactive astrocytosis that included coexpression of nestin and Gfap, and in some cases, the presence of infiltrating microglia.

Increased Proliferation of Pten-Deficient Astrocytes *In vitro* and *In vivo*. We next assessed the effects of Pten loss on astrocyte proliferation in primary cortical astrocyte cultures. Astrocyte proliferation in culture was determined at passage 2 by direct counting. The experiment shown in Fig. 5*A* is representative of growth curves evaluated from astrocyte cultures established from a total of 6 *Pten*$^{loxP/loxP}$;*GFAP-Cre*, 8 *Pten*$^{+/loxP}$;*GFAP-Cre*, and 6 *Pten*$^{+/+}$;*GFAP-Cre* mice. Pten-deficient astrocytes showed higher proliferation rates and continued to proliferate at increased saturation densities, compared with wild-type and *Pten*+/− astrocytes (Fig. 5*A*). We additionally investigated proliferation *in vivo* in 2-week-old and adult (>2 months) *Pten*$^{loxP/loxP}$;*GFAP-Cre* and control mice. S-phase cells were labeled by giving mice injections with BrdU. *Pten*$^{loxP/loxP}$;*GFAP-Cre* mice showed a significant increase in the number of BrdU-positive cells compared with the normal proliferation occurring in the cerebral cortex of control mice at 2 weeks of age ($P < 0.0001$; Fig. 5*B*). Little

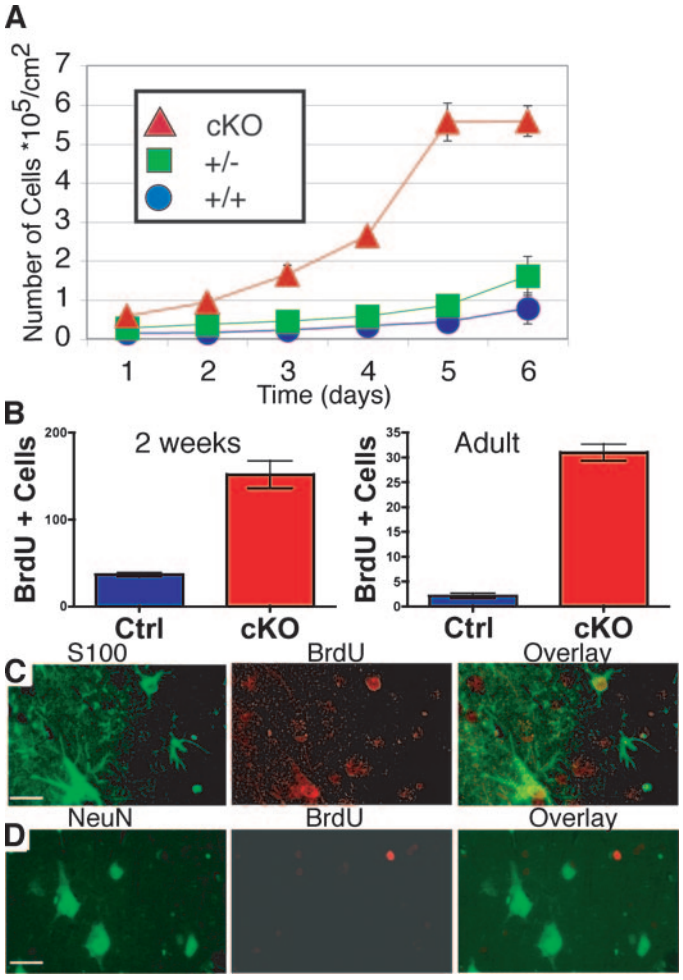

Fig. 5. Increased proliferation of *Pten*$^{loxP/loxP}$;*GFAP-Cre* astrocytes. *A*. Primary astrocyte cultures were established from *Pten*$^{loxP/loxP}$;*GFAP-Cre* mice (*cKO*), *Pten*$^{+/loxP}$;*GFAP-cre* mice (+/−), and *Pten*$^{+/+}$;*GFAP-cre* (+/+) control mice at postnatal day 2. Pten-deficient astrocytes showed a substantial proliferative advantage. Assays shown were performed in triplicate from 2 *Pten*$^{loxP/loxP}$;*GFAP-Cre* mice (▲), 3 *Pten*$^{+/loxP}$;*GFAP-cre* mice (■), and 3 *Pten*$^{+/+}$;*GFAP-cre* mice (●). *B*. Loss of Pten leads to increased glial proliferation *in vivo*. Proliferating cells were labeled by giving mice injections with BrdU. Matched sagittal sections for control and *Pten*$^{loxP/loxP}$;*GFAP-Cre* mice were subjected to BrdU immunohistochemistry, and then numbers of BrdU-positive cells in the cerebral cortex of P14 and adult mice were counted for *Pten*$^{loxP/loxP}$;*GFAP-Cre* mice (*red bars*) and control mice (*blue bars*). *A* and *B*. *Bars*, ±SD. *C*. Immunodetection of cells with BrdU incorporation and S100 expression by FITC-labeled anti-S100 (*green*) and Cy3-labeled anti-BrdU (*red*) antibodies, and the overlay of the two images. *D*. Immunodetection of cells with BrdU incorporation and NeuN expression by FITC-labeled anti-NeuN (*green*), Cy3-labeled anti-BrdU (*red*), and the overlay of the two images. Adult mice are shown in *C* and *D*. *Scale bar* = 30 μm.

proliferation was detected in the cerebral cortex of adult control animals, whereas the *Pten*$^{loxP/loxP}$;*GFAP-Cre* mice showed a significant increase in the number of cells that had entered S phase and were proliferating ($P < 0.0001$; Fig. 5*B*). We detected BrdU incorporation in cells that expressed S100β, a glial marker expressed in the nuclei and cytoplasmic projections of glia (Fig. 5*C*). In areas containing reactive astrocytes, we also detected nestin-expressing cells that incorporated BrdU (data not shown). We did not detect BrdU incorporation in neurons, identified by the neuronal marker NeuN (Fig. 5*D*).

Pten loss is also associated with changes in apoptosis in some cell types (10, 11). We performed TUNEL staining to detect apoptotic cells in control and *Pten*$^{loxP/loxP}$;*GFAP-Cre* brains from mice at P14 and adult mice. However, there was no substantial apoptosis detected in control brains, and only occasional apoptotic cells were observed in *Pten*$^{loxP/loxP}$;*GFAP-Cre* brains (data not shown). In this regard, alterations in the level of apoptosis do not account for the dramatic brain enlargement in *Pten*$^{loxP/loxP}$;*GFAP-Cre* mice.

The ongoing proliferation of glia and absence of extensive apoptosis suggested that there would be an increased number of glia in *Pten*$^{loxP/loxP}$;*GFAP-Cre* brains. The substantial hypertrophy of Pten-deficient cells resulted in a decreased cell density in *Pten*$^{loxP/loxP}$;*GFAP-Cre* mice, compared with controls (Fig. 6, *A* and *B*), that was progressive and much more pronounced in adult compared with juvenile mutant mice (data not shown). The decrease in cell density could result in a substantial underestimate of cell number if counting was performed in an area of defined size, a common approach to assess cell number. Therefore, to estimate variation in cell number, we counted cells within a defined anatomic region, which comprised a greatly enlarged area in *Pten*$^{loxP/loxP}$;*GFAP-Cre* mice. To estimate differences in the number of glia and neurons, we counted the number of cells that were immunopositive for S100, a glial marker, or NeuN, a neuronal marker. There was a significant increase in the number of S100-positive cells in the cerebral cortex of *Pten*$^{loxP/loxP}$;*GFAP-Cre* mice at P14 and in adults ($P < 0.0001$ for both age groups; Fig. 6*C*). In contrast, there was no increase in the number of NeuN-positive cells in the 2-week or adult animals (Fig. 6*D*), consistent with the absence of detectable proliferation of neurons. In fact, there was a decrease in NeuN-positive cells in adult mutant mice ($P < 0.01$), which may be accounted for by the low levels of apoptosis observed in mutant mice. Thus, increases in cell number involved glia, but not neurons.

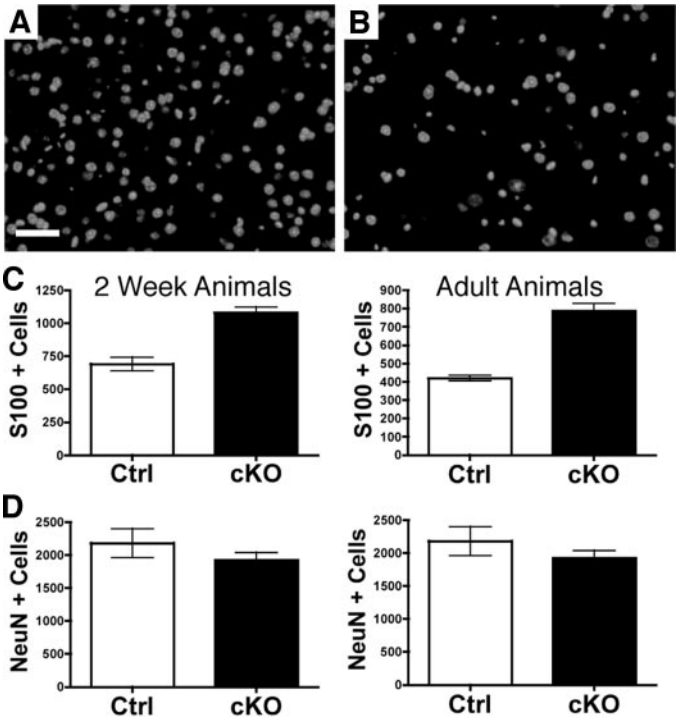

Fig. 6. Increased glial, but not neuronal, cell number in the *Pten*$^{loxP/loxP}$;*GFAP-Cre* cortex. *A* and *B*. Cell density is shown in 4′,6-diamidino-2-phenylindole stained cerebral cortex of adult control (*A*) and *Pten*$^{loxP/loxP}$;*GFAP-Cre* (*B*) mice. The increased cell size results in decreased cell density in the *Pten*$^{loxP/loxP}$;*GFAP-Cre* (*B*) compared with the control (*A*). *C*. The number of glial cells was estimated by counting S100-positive cells in the cerebral cortex of control (□) and *Pten*$^{loxP/loxP}$;*GFAP-Cre* mice (■). There are more S100-positive cells in the 2-week and adult *Pten*$^{loxP/loxP}$;*GFAP-Cre* mice compared with the control animals. *D*. The number of neurons was estimated by counting NeuN-positive cells in the cerebral cortex of the 2-week and adult animals. *Scale bar* = 50 μm for *A* and *B*. *C* and *D*. *Bars*, ±SD.

DISCUSSION

Pten function is highly dependent on the particular cell type and the specific developmental context, a feature of many tumor suppressors involved in nervous system formation and tumorigenesis. Previous studies examining the consequence of *Pten* inactivation on brain development have focused on neurons and neuroglial progenitor cells. Selective inactivation of *Pten* in neuronal cell populations during the first week of postnatal life resulted in a progressive increase in soma size without evidence of abnormal proliferation (12, 13). In contrast, Pten loss in neuroglial progenitor cells throughout the central nervous system at mid-gestation resulted in increased progenitor cell numbers, attributable to both increased proliferation and decreased cell death (apoptosis). However, ectopic proliferation was not observed in regions outside of the zones of normal progenitor cell proliferation (23).

To gain insights into the role of Pten in astroglial cell growth control and tumorigenesis, we generated mice in which *Pten* inactivation occurred in astrocytes. In this study, we show that selective deletion of *Pten* in the brain caused a dramatic hypertrophy attributed to cellular hypertrophy of astrocytes and neuronal soma, as well as enhanced and ongoing glial cell proliferation, even in the adult brain. This ongoing glial cell proliferation was seen in the adult cerebral cortex, far removed from regions where the proliferation of progenitor cells is found normally in the mature brain. In contrast, previous studies of selective neuronal *Pten* inactivation showed substantial cellular hypertrophy without ongoing proliferation in the adult brain (12, 13). This suggests that *Pten* inactivation in astroglial cells results in the generation of cell populations that continue to proliferate throughout the life of the animal and could contribute to tumor formation.

Although the primary target of Cre-mediated deletion directed by *GFAP-cre* mice was astroglia, we also observed Cre-mediated deletion in a subpopulation of neurons. We hypothesize that the neuronal *Pten* inactivation seen in our GFAP-*cre* mice reflected transient Cre expression in neuroglial progenitor cells, including radial glia. Support for the expression of GFAP in radial glial progenitor cells capable of giving rise to both neurons and astrocytes derives from studies of subventricular zone progenitor cells in the developing and adult mouse (28). Consistent with this hypothesis, several independently generated *Gfap-cre* transgenic mouse lines have exhibited various levels of Cre-mediated deletion within neuronal populations, despite the absence of ongoing Cre expression in these cells (13, 29–31). The varied extent of neuronal involvement is likely a reflection of the pool of neuroglial progenitors expressing Cre in each transgenic line. Importantly, the *GFAP-cre* transgenic line used in the present study allows analysis of Pten-deficient astrocytes in the adult cerebral hemispheres, the most common site of glioblastoma formation.

Although some of the effects observed in Pten-deficient astrocytes could be a secondary response to abnormalities within Pten-deficient neurons, three lines of evidence argue to the contrary. First, areas with reactive astrocytes and microglial invasion were distinct from the astrocytic hypertrophy observed throughout the brain. Second, proliferating astrocytes in these mice did not express protein markers (*e.g.*, nestin) associated with reactive astrocytosis. Finally, primary astrocyte cultures from these mice displayed accelerated proliferation, consistent with a cell-intrinsic defect in *Pten*-deficient astrocytes.

In addition to increased cell proliferation, we also observed a slight increase in apoptosis in adult $Pten^{loxP/loxP}$;*GFAP-Cre* brains, consistent with decreased numbers of cerebral cortical neurons in adult mutant mice. Previous studies examining the effect of *Pten* deletion in Purkinje neurons also showed progressive loss of these cells in adult mice (11). Lastly, with antisense oligonucleotide Pten suppression, loss of Pten expression in cultured central nervous system stem cells leads to the death of resulting immature neurons (32). Collectively, these observations indicate that the outcome of Pten deficiency is different between neurons and astrocytes. In this regard, the ability to promote proliferation in astrocytes, but not in neurons, likely reflects the inherent susceptibility of these two cell populations to tumorigenesis in the adult brain.

Insights into the function of Pten in regulating organ and organism size have derived from studies of the insulin signaling pathway in *Drosophila*. The insulin signaling pathway in flies is critical for controlling both cell size and cell number. Effector proteins in this pathway include homologs of genes that are targeted by mutation in human cancers, including phosphatidylinositol 3′-kinase, AKT, PTEN, and the tuberous sclerosis complex (TSC) tumor suppressors, *TSC1* and *TSC2* (33). Previously, *Tsc1* was inactivated in mice with the same *GFAP-cre* transgenic lines used in the present study. In primary astrocyte cultures, *Tsc1* deficiency showed dramatic effects on cell size but no substantial change in the proliferation of subconfluent cultures (34). In contrast, Pten-deficient primary astrocyte cultures showed increased proliferation without substantial increase in size. *In vivo*, both the *Pten* and *Tsc1* conditional knockout mice showed an overall hypertrophy of the brain and dramatic increases in Gfap-positive cells and proliferation. However, the hippocampal neuronal migration defects seen in $Pten^{loxP/loxP}$;*GFAP-Cre* mice reported herein were not observed in $Tsc1^{loxP/loxP}$;*GFAP-Cre* mice (35). In this manner, these two related mouse models provide novel experimental systems to begin to dissect the critical effectors responsible for specific defects resulting from disruption in regulation of PI3k signaling. Furthermore, these observations are relevant to human disease, because in humans, hereditary mutation of *PTEN* or *TSC1* results in the development of phenotypically distinct syndromes, in which affected patients develop multiple dysplastic hamartomatous growths (36). In light of the common downstream effectors involved in the Pten and Tsc growth regulatory pathways, previous studies have shown that *in vivo* inhibition of mTor blocks hypertrophy of Pten-deficient neurons (37) and also inhibits proliferation of Pten-deficient and Tsc-deficient tumor cells (38–40). Unique downstream effectors that discriminate between hypertrophy *versus* hyperproliferation have yet to be identified.

Although the precise relationship between cell size control and tumorigenesis remains undefined, it is interesting to note that some oncogenes that play prominent roles in cancer also influence cell size in *Drosophila*, including Myc, Ras, and Cyclin D (41). In mammalian cells, there are context-dependent influences on cell size. For example, c-Myc deficiency caused decreased body mass because of hypoproliferation without influence on cell size (42), whereas overexpression of c-Myc increased B-cell size independent of the cell cycle (43, 44). Levels of the cell cycle regulatory protein $p27^{Kip1}$ are negatively regulated by Pten and Tsc1 and Tsc2 in some, but not all, of the contexts (35, 45–49). Interestingly, $p27^{Kip1}$ regulates organ and organism size through the regulation of proliferation, but not cell size (50, 51). The regulation of cell size and cell proliferation is normally tightly coupled, with cells reaching a critical size before progressing through the cell cycle. When these processes remain coupled, increased cell growth may be instrumental in driving accelerated proliferation (33), a relationship that would clearly provide a growth advantage contributing to the development of cancer.

The contribution of PTEN inactivation to glioblastoma formation likely occurs through multiple mechanisms. Notably, the absence of *PTEN* mutations in lower grade gliomas (26) indicates that *PTEN* loss does not confer a substantial selective growth advantage early in the tumorigenic progression within the glial cell lineage. Consistent with this observation, we did not detect tumors in $Pten^{loxP/loxP}$;*GFAP-Cre* brains in which *Pten* inactivation occurs in the absence of other

tumor-associated mutations. Using glioma cell lines, it has been shown that enforced expression of PTEN results in abnormalities in cell cycle regulation, apoptosis, cell motility, angiogenesis, and regulation of metalloproteases associated with tumor cell invasion (52). However, it is unknown which of these effects of PTEN overexpression, revealed by *in vitro* manipulation of tumor cell lines, is important for glioblastoma formation *in vivo*. In a mouse model for astrocytomas, tumor development induced by inactivation of the pRb pathway in astrocytes was accelerated in $Pten^{+/-}$ mice, with an associated decrease in apoptosis (53), suggesting that Pten loss contributes to tumorigenesis *in vivo*. It is unclear whether the wild-type *Pten* allele was retained in the resulting tumors or if other functions in addition to reduced apoptosis associated with Pten deficiency also contributed to astrocytoma formation. Further studies with the mice described in this study as well as other related *Pten* conditional knockout strains will be invaluable in dissecting the various functions of Pten relevant to brain tumor formation and progression.

ACKNOWLEDGMENTS

We thank Drs. Peter Burger and Christine Fuller for insights regarding the neuropathology in our mouse model, Steven Lloyd and Dr. Richard Smeyne for assistance with Bioquant measurements, and Drs. Tom Curran, Peter McKinnon, and Dennis Steindler, and members of the Baker laboratory for helpful discussions. We appreciate the technical assistance of Junyuan Zhang and Christine Kamp.

REFERENCES

1. Ali IU, Schriml LM, Dean M. Mutational spectra of PTEN/MMAC1 gene: a tumor suppressor with lipid phosphatase activity. J Natl Cancer Inst (Bethesda) 1999;91: 1922–32.
2. Eng C. PTEN: one gene, many syndromes. Hum Mutat 2003;22:183–98.
3. Vivanco I, Sawyers CL. The phosphatidylinositol 3-kinase AKT pathway in human cancer. Nat Rev Cancer 2002;2:489–501.
4. Sulis ML, Parsons R. PTEN: from pathology to biology. Trends Cell Biol 2003;13: 478–83.
5. Freeman DJ, Li AG, Wei G, et al. PTEN tumor suppressor regulates p53 protein levels and activity through phosphatase-dependent and -independent mechanisms. Cancer Cell 2003;3:117–30.
6. Raftopoulou M, Etienne-Manneville S, Self A, Nicholls S, Hall A. Regulation of cell migration by the C2 domain of the tumor suppressor PTEN. Science (Wash DC) 2004;303:1179–81.
7. Suzuki A, de la Pompa JL, Stambolic V, et al. High cancer susceptibility and embryonic lethality associated with mutation of the PTEN tumor suppressor gene in mice. Curr Biol 1998;8:1169–78.
8. Podsypanina K, Ellenson LH, Nemes A, et al. Mutation of Pten/Mmac1 in mice causes neoplasia in multiple organ systems. Proc Natl Acad Sci USA 1999;96: 1563–8.
9. Di Cristofano A, Pesce B, Cordon-Cardo C, Pandolfi PP. Pten is essential for embryonic development and tumour suppression. Nat Genet 1998;19:348–55.
10. Groszer M, Erickson R, Scripture-Adams DD, et al. Negative regulation of neural stem/progenitor cell proliferation by the Pten tumor suppressor gene in vivo. Science (Wash DC) 2001;294:2186–9.
11. Marino S, Krimpenfort P, Leung C, et al. PTEN is essential for cell migration but not for fate determination and tumourigenesis in the cerebellum. Development (Camb) 2002;129:3513–22.
12. Backman SA, Stambolic V, Suzuki A, et al. Deletion of Pten in mouse brain causes seizures, ataxia and defects in soma size resembling Lhermitte-Duclos disease. Nat Genet 2001;29:396–403.
13. Kwon CH, Zhu X, Zhang J, et al. Pten regulates neuronal soma size: a mouse model of Lhermitte-Duclos disease. Nat Genet 2001;29:404–11.
14. Horie Y, Suzuki A, Kataoka E, et al. Hepatocyte-specific Pten deficiency results in steatohepatitis and hepatocellular carcinomas. J Clin Investig 2004;113:1774–83.
15. Kimura T, Suzuki A, Fujita Y, et al. Conditional loss of PTEN leads to testicular teratoma and enhances embryonic germ cell production. Development (Camb) 2003; 130:1691–700.
16. Li G, Robinson GW, Lesche R, et al. Conditional loss of PTEN leads to precocious development and neoplasia in the mammary gland. Development (Camb) 2002;129: 4159–70.
17. Suzuki A, Itami S, Ohishi M, et al. Keratinocyte-specific Pten deficiency results in epidermal hyperplasia, accelerated hair follicle morphogenesis and tumor formation. Cancer Res 2003;63:674–81.
18. Trotman LC, Niki M, Dotan ZA, et al. Pten dose dictates cancer progression in the prostate. PLoS Biol 2003 Dec 1;3:E59. Epub 2003 Oct 27.
19. Wang S, Gao J, Lei Q, et al. Prostate-specific deletion of the murine Pten tumor suppressor gene leads to metastatic prostate cancer. Cancer Cell 2003;4:209–21.
20. Kitange GJ, Templeton KL, Jenkins RB. Recent advances in the molecular genetics of primary gliomas. Curr Opin Oncol 2003;15:197–203.
21. Bajenaru ML, Zhu Y, Hedrick NM, et al. Astrocyte-specific inactivation of the neurofibromatosis 1 gene (NF1) is insufficient for astrocytoma formation. Mol Cell Biol 2002;22:5100–13.
22. Soriano P. Generalized lacZ expression with the ROSA26 Cre reporter strain. Nat Genet 1999;21:70–1.
23. Suzuki A, Yamaguchi MT, Ohteki T, et al. T cell-specific loss of pten leads to defects in central and peripheral tolerance. Immunity 2001;14:523–34.
24. Wechsler-Reya RJ, Scott MP. Control of neuronal precursor proliferation in the cerebellum by Sonic Hedgehog. Neuron 1999;22:103–14.
25. Novak A, Guo C, Yang W, Nagy A, Lobe CG. Z/EG, a double reporter mouse line that expresses enhanced green fluorescent protein upon Cre-mediated excision. Genesis 2000;28:147–55.
26. Silver J, Miller JH. Regeneration beyond the glial scar. Nat Rev Neurosci 2004;5: 146–56.
27. Frisen J, Johansson CB, Torok C, Risling M, Lendahl U. Rapid, widespread, and longlasting induction of nestin contributes to the generation of glial scar tissue after CNS injury. J Cell Biol 1995;131:453–64.
28. Alvarez-Buylla A, Lim DA. For the long run: maintaining germinal niches in the adult brain. Neuron 2004;41:683–6.
29. Malatesta P, Hack MA, Hartfuss E, et al. Neuronal or glial progeny: regional differences in radial glia fate. Neuron 2003;37:751–64.
30. Marino S, Vooijs M, van Der Gulden H, Jonkers J, Berns A. Induction of medulloblastomas in p53-null mutant mice by somatic inactivation of Rb in the external granular layer cells of the cerebellum. Genes Dev 2000;14:994–1004.
31. Anthony TE, Klein C, Fishell G, Heintz N. Radial glia serve as neuronal progenitors in all regions of the central nervous system. Neuron 2004;41:881–90.
32. Lachyankar MB, Sultana N, Schonhoff CM, et al. A role for nuclear PTEN in neuronal differentiation. J Neurosci 2000;20:1404–13.
33. Kozma SC, Thomas G. Regulation of cell size in growth, development and human disease: PI3K, PKB and S6K. Bioessays 2002;24:65–71.
34. Uhlmann EJ, Li W, Scheidenhelm DK, et al. Loss of tuberous sclerosis complex 1 (Tsc1) expression results in increased Rheb/S6K pathway signaling important for astrocyte cell size regulation. Glia 2004;47:180–88.
35. Uhlmann EJ, Wong M, Baldwin RL, et al. Astrocyte-specific TSC1 conditional knockout mice exhibit abnormal neuronal organization and seizures. Ann Neurol 2002;52:285–96.
36. Barker KT, Houlston RS. Overgrowth syndromes: is dysfunctional PI3-kinase signalling a unifying mechanism? Eur J Hum Genet 2003;11:665–70.
37. Kwon CH, Zhu X, Zhang J, Baker SJ. mTor is required for hypertrophy of Pten-deficient neuronal soma in vivo. Proc Natl Acad Sci USA 2003;100:12923–8.
38. Podsypanina K, Lee RT, Politis C, et al. An inhibitor of mTOR reduces neoplasia and normalizes p70/S6 kinase activity in Pten+/− mice. Proc Natl Acad Sci USA 2001;98:10320–5.
39. Neshat MS, Mellinghoff IK, Tran C, et al. Enhanced sensitivity of PTEN-deficient tumors to inhibition of FRAP/mTOR. Proc Natl Acad Sci USA 2001;98:10314–9.
40. Kenerson HL, Aicher LD, True LD, Yeung RS. Activated mammalian target of rapamycin pathway in the pathogenesis of tuberous sclerosis complex renal tumors. Cancer Res 2002;62:5645–50.
41. Potter CJ, Xu T. Mechanisms of size control. Curr Opin Genet Dev 2001;11:279–86.
42. Trumpp A, Refaeli Y, Oskarsson T, et al. c-Myc regulates mammalian body size by controlling cell number but not cell size. Nature (Lond) 2001;414:768–73.
43. Iritani BM, Eisenman RN. c-Myc enhances protein synthesis and cell size during B lymphocyte development. Proc Natl Acad Sci USA 1999;96:13180–5.
44. Schuhmacher M, Staege MS, Pajic A, et al. Control of cell growth by c-Myc in the absence of cell division. Curr Biol 1999;9:1255–8.
45. Mamillapalli R, Gavrilova N, Mihaylova VT, et al. PTEN regulates the ubiquitin-dependent degradation of the CDK inhibitor p27(KIP1) through the ubiquitin E3 ligase SCF(SKP2). Curr Biol 2001;11:263–7.
46. Zhu X, Kwon CH, Schlosshauer PW, Ellenson LH, Baker SJ. PTEN induces G(1) cell cycle arrest and decreases cyclin D3 levels in endometrial carcinoma cells. Cancer Res 2001;61:4569–75.
47. Nakamura N, Ramaswamy S, Vazquez F, et al. Forkhead transcription factors are critical effectors of cell death and cell cycle arrest downstream of PTEN. Mol Cell Biol 2000;20:8969–82.
48. Uhlmann EJ, Apicelli AJ, Baldwin RL, et al. Heterozygosity for the tuberous sclerosis complex (TSC) gene products results in increased astrocyte numbers and decreased p27-Kip1 expression in TSC2+/− cells. Oncogene 2002;21:4050–9.
49. Soucek T, Rosner M, Miloloza A, et al. Tuberous sclerosis causing mutants of the TSC2 gene product affect proliferation and p27 expression. Oncogene 2001;20: 4904–9.
50. Fero ML, Rivkin M, Tasch M, et al. A syndrome of multiorgan hyperplasia with features of gigantism, tumorigenesis, and female sterility in p27(Kip1)-deficient mice. Cell 1996;85:733–44.
51. Nakayama K, Ishida N, Shirane M, et al. Mice lacking p27(Kip1) display increased body size, multiple organ hyperplasia, retinal dysplasia, and pituitary tumors. Cell 1996;85:707–20.
52. Konopka G, Bonni A. Signaling pathways regulating gliomagenesis. Curr Mol Med 2003;3:73–84.
53. Xiao A, Wu H, Pandolfi PP, Louis DN, Van Dyke T. Astrocyte inactivation of the pRb pathway predisposes mice to malignant astrocytoma development that is accelerated by PTEN mutation. Cancer Cell 2002;1:157–68.